

# Three-dimensional Skyrme Hartree-Fock-Bogoliubov solver in coordinate-space representation

Mengzhi Chen<sup>a,b,\*</sup>, Tong Li<sup>a,b</sup>, Bastian Schuetrumpf<sup>a</sup>, Paul-Gerhard Reinhard<sup>c</sup>, Witold Nazarewicz<sup>a,b</sup>

<sup>a</sup>*Facility for Rare Isotope Beams, Michigan State University, East Lansing, Michigan 48824, USA*

<sup>b</sup>*Department of Physics and Astronomy, Michigan State University, East Lansing, Michigan 48824, USA*

<sup>c</sup>*Institut für Theoretische Physik, Universität Erlangen, D-91054 Erlangen, Germany*

## Abstract

The coordinate-space representation of the Hartree-Fock-Bogoliubov theory is the method of choice to study weakly bound nuclei whose properties are affected by the quasiparticle continuum space. To describe such systems, we developed a three-dimensional Skyrme-Hartree-Fock-Bogoliubov solver HFBFFT based on the existing, highly optimized and parallelized Skyrme-Hartree-Fock code SKY3D. The code does not impose any self-consistent spatial symmetries such as mirror inversions or parity. The underlying equations are solved in HFBFFT directly in the canonical basis using the fast Fourier transform. To remedy the problems with pairing collapse, we implemented the soft energy cutoff and pairing annealing. The convergence of HFB solutions was improved by a sub-iteration method. The Hermiticity violation of differential operators brought by Fourier-transform-based differentiation has also been solved. The accuracy and performance of HFBFFT were tested by benchmarking it against other HFB codes, both spherical and deformed, for a set of nuclei, both well-bound and weakly-bound.

**Keywords:** Nuclear Density Functional Theory; Hartree-Fock-Bogoliubov method; Skyrme energy density functional; Finite volume methods; 3D coordinate-space representation

## 1. Introduction

Exotic nuclei with extreme neutron-to-proton ratios are crucial for theoretical nuclear structure research as their properties provide critical information on nuclear interactions, many-body techniques, and astrophysical scenarios. However, because of their weak binding, their quasiparticle excitations are often affected by the low-lying scattering space (a.k.a. particle continuum), which enhances the necessary computational effort. For such nuclei, nucleonic pairing must be handled within the full Hartree-Fock-Bogoliubov (HFB) scheme instead of the simpler Bardeen-Cooper-Schrieffer (BCS) approximation [1, 2, 3, 4, 5]. In addition, the associated self-consistent densities are usually very extended in space, which requires large basis sets or large coordinate-space boxes. Both requirements become particularly demanding if one aims at symmetry-unrestricted calculations (i.e., without imposing space reflection or axial or spherical symmetries). The paper aims to propose a reliable and efficient computational scheme to solve the HFB equations on a three-dimensional (3D) Cartesian coordinate-space grid.

The nuclear energy density functional (EDF) method is one of the most widely used methods to study medium-mass and heavy nuclei [6, 7]. Its main ingredient is an EDF that represents the effective in-medium nuclear interaction. Among many

EDFs, the Skyrme functional, originally based on Skyrme interaction [8], is commonly used to study global nuclear properties, such as ground-state energies, deformations, and low-lying excitations [7, 9, 10]. It is to be noted that the nuclear EDF method is closely related to the density-functional theory (DFT). Hence, it is often referred to as nuclear DFT.

Over the years, a number of HFB solvers have been developed; see Table 2 of Ref. [11] for a summary. These solvers can be divided into two families. The codes in the first group are based on the expansion of single-particle wave functions in a finite set of basis functions such as the harmonic oscillator (HO) eigenfunctions. Examples of such solvers are: HFBTHO [12, 13], which solves the axial (2D) HFB equations in the axial HO or the transformed HO basis; HFODD [14, 15, 16], which solves the 3D HFB equations in the Cartesian HO basis without assumption of self-consistent symmetries; and HFBPTG [17], which solves the axial (2D) HFB equations in the Pöschl-Teller-Ginocchio basis.

The basis-expansion method is efficient and has been successfully employed in large-scale calculations [10]. However, when it is applied to weakly-bound nuclei, the performance of this method deteriorates as huge configuration spaces are required to describe the asymptotic behavior of HFB solutions. Here, the approach of choice is the HFB framework formulated in the coordinate-space representation [1, 3, 4].

The coordinate-space solvers constitute the second family of HFB codes. Examples of such solvers are: HFBRAD [18] solves spherically symmetric HFB problem using finite differences; HFB-AX [19] is a 2D solver based on B-splines;

\*Corresponding author

Email addresses: chenme24@msu.edu (Mengzhi Chen), lit@nsl.msui.edu (Tong Li), bastian.schuetrumpf@gmail.com (Bastian Schuetrumpf), Paul-Gerhard.Reinhard@fau.de (Paul-Gerhard Reinhard), witek@frib.msui.edu (Witold Nazarewicz)

SKYAX [20] is a highly optimized 2D Hartree-Fock (HF) + BCS code using the fast Fourier transform (FFT) method to compute derivatives; SKY3D [21, 22] is a 3D extension of SKYAX; the predecessor of SKYAX and SKY3D is a 1D spherical HF+BCS code using five-point finite differences which was published first in [23] and has meanwhile been developed into a full spherical HFB code SKY1D [24]; the HFB extension of SKYAX is SKY2D [24]; EV8 solves the Skyrme HF+BCS equations using the imaginary time method on a 3D mesh that is limited to one octant by imposing time-reversal and spatial symmetries [25, 26]; MOCCA [27, 28] is a Skyrme-HFB extension of EV8; MADNESS-HFB [29] is a 3D HFB solver based on multi-resolution analysis and multi-wavelet expansion; LISE is a 3D HFB solver [30] employing the discrete variable representation (or Lagrange-mesh method) and fast Fourier transforms; and there are also 3D HFB solvers based on the contour integral of the Green's function using the shifted Krylov subspace method [31, 32].

The major difference between basis-based and mesh-based methods is the treatment of one-quasiparticle continuum space [2, 33, 34, 4]. In the case of coordinate-space methods, the discretized continuum strongly depends on the geometry of the spatial box and the grid size. For large 3D boxes and dense grids, the size of the discretized continuum space quickly becomes intractable as the maximum allowed quasiparticle energy increases.

A promising approach to the coordinate-space HFB problem is the canonical-basis HFB method proposed in Refs. [35, 36]. The one-body density matrix is diagonal in the canonical basis (or natural orbits), and its eigenstates are spatially localized if the nucleus is particle-bound. Because of this localization, the single-particle (s.p.) continuum level density is significantly reduced.

In this work, we develop a 3D Skyrme-HFB solver HFBFFT in the coordinate-space representation. This code is based on the published code SKY3D [21, 22]. SKY3D has been well optimized for performance and parallelized with OpenMP and MPI [37]. In HFBFFT we maintain the high-level parallelization, making it scalable on modern supercomputers. In order to overcome the pairing collapse problem mentioned in Ref. [36], we implement the soft energy cutoff of pairing space and develop the annealing of pairing strengths to avoid pairing deadlock at an early stage. Furthermore, we introduce the sub-iteration method in the configuration space to stabilize and speed up the convergence. We also resolve the problem of Hermiticity violation in SKY3D brought by the incompatibility between the product rule and the Fourier-transform-based algorithm for derivatives. To benchmark HFBFFT we study several nuclear systems and compare our results against HFBTHO and the coordinate-space HFB codes SKY1D and SKY2D, which solve the HFB problem in 1D (spherical) and 2D (axial) geometries, respectively.

This paper is organized as follows. In Sec. 2, the Skyrme EDF and the HFB theory are briefly introduced. The numerical details and algorithms of HFBFFT are described in section 3. In Sec. 4, we present test and benchmark results. Finally, conclusions and outlooks are presented in Sec. 5.

## 2. Skyrme Hartree-Fock-Bogoliubov theory

In this section, we briefly summarize the Skyrme EDF and the HFB theory.

### 2.1. The Skyrme energy density functional

The HFB theory describes a many-Fermion system in terms of an orthonormal set of s.p. wave functions  $\psi_\alpha$  with fractional occupation amplitudes  $v_\alpha$ , i.e.,

$$\{\psi_\alpha, v_\alpha, \alpha = 1, \dots, \Omega\}, \quad (1)$$

where  $\Omega$  denotes the size of the active s.p. space. The amplitude  $v_\alpha$  can take values continuously in the interval  $[0, 1]$ . The complementary amplitude is  $u_\alpha = \sqrt{1 - v_\alpha^2}$ .

The code HFBFFT uses a formulation of HFB theory in the basis of natural orbitals, which are defined as the basis of s.p. states  $\psi_\alpha$  in which the one-body density matrix  $\hat{\rho}$  is diagonal, i.e.,  $\hat{\rho} = \sum_\alpha |\psi_\alpha\rangle n_\alpha \langle\psi_\alpha|$ , where  $n_\alpha$ , an eigenvalue of  $\hat{\rho}$ , represents the canonical-state occupation. The numerical HFB scheme in the canonical basis was presented in [35] and improved in [36]. For the relation between the standard matrix formulation and the canonical formulation of HFB, see Refs. [3, 38]. In the canonical basis, the HFB mean-field state takes the BCS-like form:

$$|\Phi\rangle = \prod_{\alpha>0} (u_\alpha + v_\alpha \hat{a}_\alpha^\dagger \hat{a}_{\bar{\alpha}}^\dagger) |0\rangle \quad (2)$$

where  $|0\rangle$  is the vacuum state,  $\hat{a}_\alpha^\dagger$  is the creation operator of  $\psi_\alpha$ , and  $\bar{\alpha}$  the conjugate partner to state  $\alpha$  that corresponds to the same eigenvalue of  $\hat{\rho}$ .

Any self-consistent mean-field theory starts from expressing the energy of the system in terms of s.p. wave functions and occupation amplitudes (1). EDFs go for a simpler approach by starting from the energy defined in terms of only a few local densities and currents. For the case of stationary states of even-even nuclei, the energy depends only on the local particle density  $\rho_q$ , the kinetic-energy density  $\tau_q$ , and the spin-orbit density  $J_q$ :

$$\begin{aligned} \rho_q(\mathbf{r}) &= \sum_{\alpha \in q} \sum_s v_\alpha^2 |\psi_\alpha(\mathbf{r}, s)|^2, \\ \tau_q(\mathbf{r}) &= \sum_{\alpha \in q} \sum_s v_\alpha^2 |\nabla \psi_\alpha(\mathbf{r}, s)|^2, \\ J_q(\mathbf{r}) &= -i \sum_{\alpha \in q} \sum_{ss'} v_\alpha^2 \psi_\alpha^*(\mathbf{r}, s) \nabla \times \boldsymbol{\sigma}_{ss'} \psi_\alpha(\mathbf{r}, s'), \end{aligned} \quad (3a)$$

where  $q \in \{p, n\}$  stands for protons or neutrons and  $s, s' = \pm 1/2$  label the two spinor components of the wave functions. Pairing EDFs additionally require the pairing density

$$\xi_q(\mathbf{r}) = \sum_{\alpha \in q}^{(\text{cut})} u_\alpha v_\alpha \sum_s (-2s) \psi_{\bar{\alpha}}(\mathbf{r}, -s) \psi_\alpha(\mathbf{r}, s), \quad (3b)$$

where the first summation includes a cutoff in the pairing space. For a stationary state of an even-even nucleus, the conjugate s.p. state  $\bar{\alpha}$  can be assumed to be the time-reversed state of  $\alpha$ , which

leads to

$$\xi_q(\mathbf{r}) = \sum_{\alpha \in q} \sum_s^{(\text{cut})} u_\alpha v_\alpha |\psi_\alpha(\mathbf{r}, s)|^2. \quad (3c)$$

The code HFBFFT, as its predecessor SKY3D, employs the widely used Skyrme EDF. This EDF is well described in all details at several places [6, 9, 7]. Thus we give here only a brief account with emphasis on the pairing part. The total energy is a functional of the local densities:

$$E_{\text{tot}} = E_{\text{Skyrme}}[\rho, \tau, \mathbf{J}] + E_{\text{pair}}[\rho, \xi] + E_{\text{Coul}}[\rho_p], \quad (4a)$$

where (ignoring here isospin index for simplicity)

$$\begin{aligned} E_{\text{Skyrme}} &= E_{\text{kin}} + E_{\rho\rho} + E_{\rho\tau} + E_{\rho\Delta\rho} + E_{\nabla\mathbf{J}} \\ &= \int d^3r \left[ \frac{\hbar^2}{2m} \tau + C^\rho \rho^2 + C^\tau \rho\tau + C^{\Delta\rho} \rho\Delta\rho + C^J \rho \nabla \cdot \mathbf{J} \right], \end{aligned} \quad (4b)$$

$$E_{\text{pair}} = \frac{1}{4} \sum_{q \in \{p, n\}} V_{\text{pair}, q} \int d^3r |\xi_q|^2 \left[ 1 - \frac{\rho}{\rho_{0, \text{pair}}} \right], \quad (4c)$$

$$E_{\text{Coul}} = \frac{e^2}{2} \int d^3r d^3r' \frac{\rho_p(\mathbf{r})\rho_p(\mathbf{r}')}{|\mathbf{r} - \mathbf{r}'|} - \int d^3r \frac{3e^2}{4} \left( \frac{3}{\pi} \right)^{\frac{1}{3}} \rho_p^{4/3}. \quad (4d)$$

$E_{\text{Skyrme}}$  is a functional of  $\rho$ ,  $\tau$ , and  $\mathbf{J}$ ;  $E_{\text{pair}}$  is a functional of  $\rho$  and  $\xi$ ; and the Coulomb energy  $E_{\text{Coul}}$  is a functional of proton density  $\rho_p$ . The pairing functional can be motivated by a density-dependent  $\delta$  interaction. It includes two limiting cases. The first case is a pure contact interaction, also called volume pairing, which is recovered when  $\rho_{0, \text{pair}} \rightarrow \infty$ . The second case corresponds to a value near matter equilibrium density  $\rho_{0, \text{pair}} = 0.16 \text{ fm}^{-3}$ , which localizes pairing around the nuclear surface. Adjustment of  $\rho_{0, \text{pair}}$  as a free parameter delivers a form of the pairing functional which stays in between the extremes of volume and surface pairing [39, 40].

## 2.2. The HFB theory in canonical basis

In practice, one deals with two types of fermions: protons and neutrons. To keep the notation simple, in the following, we assume that the isospin quantum number is included in the quantum label  $\alpha$  of the canonical state. The HFB equations are derived variationally by minimizing the HFB Routhian

$$R = E_{\text{tot}} - \sum_{q \in \{p, n\}} \epsilon_{F, q} \sum_{\alpha \in q} v_\alpha^2 - \sum_{\alpha\beta} \lambda_{\alpha\beta} (\langle \psi_\beta | \psi_\alpha \rangle - \delta_{\alpha\beta}), \quad (5)$$

with respect to  $\psi_\alpha$  and  $v_\alpha$ . In Eq. (5)  $\epsilon_F$  is the Fermi energy which is also the Lagrange parameter for the particle-number constraint, and the  $\hat{\lambda}$  is the matrix of Lagrangian multipliers that guarantee the orthonormality of canonical wave functions. Since  $\langle \psi_\beta | \psi_\alpha \rangle = \langle \psi_\alpha | \psi_\beta \rangle^*$ , it is required that the matrix  $\hat{\lambda}$  is Hermitian so that the number of its independent elements coincides with the total number of independent constraints.

Variation of the Skyrme and Coulomb energies with regard

to the s.p. wave function yields the HF Hamiltonian  $\hat{h}$ :

$$\frac{\delta (E_{\text{Skyrme}} + E_{\text{Coul}})}{\delta \psi_\alpha^\dagger} = v_\alpha^2 \hat{h} \psi_\alpha. \quad (6)$$

By the chain rule for derivatives, (6) can be reduced to the variation with respect to the densities, which delivers explicit expressions for  $\hat{h}$  [6, 9]. The HF Hamiltonian  $\hat{h}$  is a functional of local densities (particle density, kinetic-energy density, spin-orbit density) in the standard fashion of nuclear EDFs [6].

Variation of the pairing energy with respect to the s.p. wave function gives

$$\frac{\delta E_{\text{pair}}}{\delta \psi_\alpha^\dagger} = u_\alpha v_\alpha \hat{h} \psi_\alpha + v_\alpha^2 \hat{h}' \psi_\alpha. \quad (7)$$

The first term is related to the variation with respect to the pairing density, which yields the pairing potential [38]

$$\tilde{h}_q(\mathbf{r}) = \frac{1}{2} V_{\text{pair}, q} \xi_q \left[ 1 - \frac{\rho}{\rho_{0, \text{pair}}} \right], \quad q \in \{p, n\}. \quad (8)$$

The second term is the pairing-rearrangement term, brought by the density dependence of the pairing functional. For simplicity, we treat the rearrangement term  $\hat{h}'$  as part of the HF Hamiltonian  $\hat{h}$  in the following. The pairing potential  $\tilde{h}_q(\mathbf{r})$  is a local potential in most pairing functionals. From that, we obtain the state-dependent gap

$$\Delta_{\alpha\alpha} = \langle \psi_\alpha | \tilde{h}_{q_\alpha} | \psi_\alpha \rangle, \quad (9)$$

where  $q_\alpha$  is the isospin of state  $\alpha$ . Another aspect of the pairing is determined by the gap equation, which is obtained from the variation with respect to  $v_\alpha$ :

$$0 = 4v_\alpha (h_{\alpha\alpha} - \epsilon_{F, q_\alpha}) + 2 \left( \frac{v_\alpha^2}{u_\alpha} - u_\alpha \right) \Delta_{\alpha\alpha}, \quad (10)$$

where  $h_{\alpha\alpha}$  are the diagonal matrix elements of the HF Hamiltonian  $\hat{h}$ . The HF Hamiltonian together with the pairing potential constitutes the main ingredients of the HFB equations.

With the orthonormality of canonical states taken into account, the constrained variation of the total energy with respect to  $\psi_\alpha^\dagger$  yields the mean-field equations:

$$\hat{\mathcal{H}}_\alpha \psi_\alpha = \sum_\beta \psi_\beta \lambda_{\beta\alpha}, \quad (11)$$

where

$$\hat{\mathcal{H}}_\alpha = v_\alpha^2 \hat{h} + u_\alpha v_\alpha \hat{h}', \quad (12a)$$

$$\lambda_{\beta\alpha} = \frac{1}{2} \langle \psi_\beta | \hat{\mathcal{H}}_\alpha + \hat{\mathcal{H}}_\beta | \psi_\alpha \rangle. \quad (12b)$$

The mean-field equations (11,12) and gap equations (10) together constitute the self-consistent HFB equations in the canonical basis.

In (12a)  $\hat{\mathcal{H}}_\alpha$  is a state-dependent one-body Hamiltonian composed of the HF Hamiltonian and the pairing potential. The full matrix  $\hat{\lambda}$  needs to be taken into account because the  $\hat{\mathcal{H}}_\alpha$  are

state-dependent [35, 36]. In contrast, pure HF or HF+BCS calculations only require diagonal matrix elements  $\lambda_{\alpha\alpha}$ , which are also known as s.p. energies. The Hermiticity of  $\hat{\lambda}$  is enforced by explicit symmetrization in Eq. (12b). It can be shown by multiplying both sides of Eq. (11) by  $\psi_\beta^\dagger$  that the final solution should obey the symmetry conditions

$$0 = \lambda_{\beta\alpha}^- \equiv \frac{1}{2} \left( \langle \psi_\beta | \hat{\mathcal{H}}_\alpha | \psi_\alpha \rangle - \langle \psi_\beta | \hat{\mathcal{H}}_\beta | \psi_\alpha \rangle \right). \quad (13a)$$

One can combine these into one condition:

$$0 = \Delta S^2 \equiv \frac{1}{\Omega^2} \sum_{\alpha\beta} |\lambda_{\beta\alpha}^-|^2, \quad (13b)$$

which is the average of squared matrix elements of  $\hat{\lambda}^-$ . The actual size of  $\Delta S^2$  will serve as a check for the convergence of the HFB solution.

It should be noted that  $\hat{\lambda}^-$  vanishes when both s.p. states  $\psi_\alpha$  and  $\psi_\beta$  are fully occupied ( $v_\alpha = v_\beta = 1$ ) or unoccupied ( $v_\alpha = v_\beta = 0$ ) since then  $\langle \psi_\alpha | \hat{h} | \psi_\beta \rangle = \langle \psi_\beta | \hat{h} | \psi_\alpha \rangle^*$ . Thus, for a pure HF calculation,  $\Delta S^2$  measures the overlap between occupied and unoccupied orbits, which should be zero at the self-consistent solution.

When the size of active s.p. space equals the number of particles ( $\Omega_n = N$ ,  $\Omega_p = Z$ ) and all the s.p. orbits are fully occupied (as in the pure HF calculation),  $\Delta S^2$  is always zero; hence, it is not an appropriate measure for convergence. However, this quantity can still be utilized to check the Hermiticity of our implementation of  $\hat{h}$  (see Sec. 3.6). For the pure HF case, a suitable quantity for convergence check could be

$$\sum_\alpha |\langle \psi_\alpha | \hat{h}^2 | \psi_\alpha \rangle - \langle \psi_\alpha | \hat{h} | \psi_\alpha \rangle^2|, \quad (14)$$

which is zero at the HF solution.

### 3. Numerical representation

#### 3.1. Numerical realization on a 3D coordinate-space grid

The numerical representation is explained in detail in Refs. [21, 22]. Here, we repeat the essentials briefly. For simplicity, our discretization strategy is explained here for one dimension; the generalization to 3D is straightforward.

All wave functions, densities and fields are defined on a three-dimensional equidistant Cartesian grid. The grid points in the  $x$  direction are

$$x_\nu = \left( -\frac{N_x + 1}{2} + \nu \right) \delta x, \quad \nu = 1, \dots, N_x, \quad (15)$$

where  $N_x$  is the (even) number of grid points and  $\delta x$  is the grid spacing. Similar gridding applies to the  $y$  and  $z$  directions. The action of local operators on a coordinate-space grid is a simple multiplication of the local operator field and the wave function. The action of momentum operators, such as in the kinetic energy, requires first and second derivatives defined in Fourier space. The Fourier technique has been proved to be superior in

precision and advantageous for large grids [41]. It is noteworthy that the direct Coulomb potential is also solved in Fourier space. The Coulomb solver has to fulfill the condition that the result in the box is the correct solution to Poisson's equation with the boundary condition of zero potential at infinity. The algorithm to solve Poisson's equation for an isolated charged distribution has been implemented in SKY3D. It follows the ideas of [42, 43] by doubling the 3D grid, folding the proton density with the  $1/r$  Green's function in momentum space and then restricting the final solution inside the original box.

The discrete grid points  $k_n$  in Fourier space are related to the same number of grid points  $x_\nu$  in coordinate space as:

$$k_n = \begin{cases} (n-1)\delta k, & n = 1, \dots, \frac{N_x}{2} \\ (n - N_x - 1)\delta k, & n = \frac{N_x}{2} + 1, \dots, N_x \end{cases}, \quad (16a)$$

$$\delta k = \frac{2\pi}{N_x \delta x}. \quad (16b)$$

Note that the coordinate-space grid (15) in combination with the conjugate momentum-space grid (16), imposes no spatial symmetry at all. But the particular examples considered for benchmarking in this study obey reflection symmetry in all three directions.

A wave function  $\psi(x_\nu)$  in coordinate space is related to a wave function  $\tilde{\psi}(k_n)$  in Fourier space by the discrete Fourier transform and its inverse

$$\tilde{\psi}(k_n) = \sum_{\nu=1}^{N_x} \exp(-ik_n x_\nu) \psi(x_\nu), \quad (17a)$$

$$\psi(x_\nu) = \frac{1}{N_x} \sum_{n=1}^{N_x} \exp(ik_n x_\nu) \tilde{\psi}(k_n). \quad (17b)$$

Both can be efficiently computed via the FFT algorithm provided by the FFTW3 library [44]. This complex Fourier representation implies that the function  $\psi$  is periodic, i.e.,  $\psi(x + N_x \cdot \delta x) = \psi(x)$ . The appropriate integration scheme that complies with the above summations is the trapezoidal rule

$$\int_{-\frac{N_x}{2}\delta x}^{\frac{N_x}{2}\delta x} dx f(x) \approx \sum_{\nu=1}^{N_x} f(x_\nu) \delta x, \quad (18)$$

where all terms are added up with equal weights.

In Fourier space the  $m$ -th derivative becomes a multiplication by  $(ik_n)^m$ . One proceeds then in the following way: First, a forward transform (17a) is performed; then  $\tilde{\psi}(k_n)$  is multiplied by  $(ik_n)^m$ ; and finally  $(ik_n)^m \tilde{\psi}(k_n)$  is transformed back to the coordinate space by Eq. (17b). One should note that there is an arbitrariness about the choice of momentum  $k_{N_x/2+1}$ : it can be taken as  $\pm \frac{N_x}{2} \delta k$ . This arbitrariness does not alter the transforms (17a, 17b) but gives different results of the  $m$ -th derivative when  $m$  is odd (no impact when  $m$  is even). A natural choice is to equally split  $\tilde{\psi}(k_{N_x/2+1})$  between the positive and negative momenta, making them cancel each other in the final result of an odd-order derivative. It is equivalent to setting  $\tilde{\psi}(k_{N_x/2+1}) = 0$ .

This choice ensures that the derivative of a real-valued function is still real-valued; it also means that the second derivative is not equivalent to two consecutive first derivatives in this framework. The remaining problem is the Hermiticity breaking caused by the product rule; we will discuss it in Sec. 3.6.

### 3.2. Solution by accelerated gradient iteration

The solution of the coupled HFB equations (2.2) is obtained by interlaced iterations of the gap equation and the mean-field equation. The gap equation (10) can be solved in a closed form and it yields:

$$\begin{Bmatrix} v_\alpha \\ u_\alpha \end{Bmatrix} = \sqrt{\frac{1}{2} \mp \frac{1}{2} \frac{h_{\alpha\alpha} - \epsilon_{F,q\alpha}}{\sqrt{(h_{\alpha\alpha} - \epsilon_{F,q\alpha})^2 + \Delta_{\alpha\alpha}^2}}}. \quad (19)$$

The Fermi energy  $\epsilon_F$  needs to be adjusted to fulfill the particle-number condition

$$\epsilon_{F,q} \longleftrightarrow \sum_{\alpha \in q} v_\alpha^2 = N_q, \quad (20)$$

where  $N_q$  is the required particle number. Note that only the diagonal elements of the pairing potential and the HF Hamiltonian in the canonical basis enter (19); hence, no information about the non-diagonal elements is needed to determine the occupation amplitudes.

The solution of the mean-field equation (11) is obtained by the damped gradient iteration [21, 45, 41] interlaced with updating the matrix  $\hat{\lambda}$  for the orthonormality constraint. The steps are:

1. For given  $\{\psi_\alpha, v_\alpha, u_\alpha, \alpha = 1, \dots, \Omega\}$  compute the local densities, the HF Hamiltonian  $\hat{h}$  and the pairing potential  $\hat{h}$ .
2. Compute the action of  $\hat{h}$  and  $\hat{h}$  on all  $\psi_\alpha$  and store the result in work arrays  $\Psi_\alpha$  and  $\tilde{\Psi}_\alpha$ , i.e.,

$$\hat{h}\psi_\alpha \longrightarrow \Psi_\alpha, \quad (21a)$$

$$\hat{h}\psi_\alpha \longrightarrow \tilde{\Psi}_\alpha, \quad (21b)$$

for  $\alpha = 1, \dots, \Omega$ .

3. Use  $\Psi_\alpha$  and  $\tilde{\Psi}_\alpha$  to compute and store the s.p. energies and pairing gaps

$$h_{\alpha\alpha} = \langle \psi_\alpha | \Psi_\alpha \rangle, \quad (22a)$$

$$\Delta_{\alpha\alpha} = \langle \psi_\alpha | \tilde{\Psi}_\alpha \rangle. \quad (22b)$$

4. Evaluate and store the action of the generalized mean-field Hamiltonian (overwriting  $\Psi_\alpha$ )

$$\mathcal{H}_\alpha \psi_\alpha = v_\alpha^2 \Psi_\alpha + u_\alpha v_\alpha \tilde{\Psi}_\alpha \longrightarrow \Psi_\alpha. \quad (23)$$

5. Apply the matrix of Lagrange multipliers on all  $\psi_\alpha$ ; compute and store (again overwriting  $\Psi_\alpha$ )

$$\Psi_\alpha - \sum_\beta \psi_\beta \lambda_{\beta\alpha} \longrightarrow \Psi_\alpha. \quad (24)$$

6. Apply the damping operation  $\hat{\mathcal{D}}$  and orthonormalization  $\hat{\mathcal{O}}$

$$\psi_\alpha^{(\text{new})} = \hat{\mathcal{O}} \{ \psi_\alpha - \hat{\mathcal{D}} \psi_\alpha \}, \quad (25a)$$

$$\hat{\mathcal{D}} = \frac{x_0}{v_\alpha^2 (\hat{T} + E_0) + \frac{1}{2} u_\alpha v_\alpha \tilde{h}_0}, \quad (25b)$$

where  $x_0$ ,  $E_0$ , and  $\tilde{h}_0$  are adjustable numerical parameters. The empirical values  $x_0 = 0.45$ ,  $E_0 = 100$  MeV and  $\tilde{h}_0 = \max [\tilde{h}_n(\mathbf{r}), \tilde{h}_p(\mathbf{r})]$  are used in our calculations. It is worth noting that the lower bound of  $u_\alpha v_\alpha$  and  $v_\alpha^2$  in  $\hat{\mathcal{D}}$  is set to be  $10^{-1}$  for numerical stability.

7. With the new  $h_{\alpha\alpha}$  and  $\Delta_{\alpha\alpha}$  from step 3, compute new occupations  $v_\alpha$  and  $u_\alpha$  using Eq. (19).
8. Reevaluate the action of the generalized mean-field Hamiltonian on all  $\psi_\alpha$  and compute the matrix of Lagrange multipliers

$$\lambda_{\beta\alpha} = \frac{\langle \psi_\beta | \hat{\mathcal{H}}_\alpha | \psi_\alpha \rangle + \langle \psi_\alpha | \hat{\mathcal{H}}_\beta | \psi_\beta \rangle^*}{2}. \quad (26)$$

The above iteration usually starts from a number of HF+BCS steps, which are done in the same way as in SKY3D. The HF+BCS calculation is initialized by a 3D HO wave function that can be triaxially deformed. To achieve better convergence, in step 1 the new densities are mixed linearly with the old ones:

$$\kappa^{(n)} = (1 - \gamma) \kappa^{(n-1)} + \gamma \kappa_\psi^{(n)}, \quad \kappa = \rho, \tau \text{ or } \xi, \quad (27)$$

where  $n$  is the iteration number, subscript  $\psi$  denotes the density directly computed from the wave functions, and  $\gamma$  is the adjustable mixture ratio with a default value of 0.2.

### 3.3. Sub-iterations in configuration space

The damped gradient scheme outlined in Sec. 3.2 converges, but requires more iterations in the HFB scheme as compared to the HF + BCS used in SKY3D. It also involves operations on the full 3D grid which can make computations cumbersome. The pairing part in the iterative steps works predominantly within the given space of canonical states. Thus one can reduce the total numerical expense by the sub-iteration method: switching between the full 3D step and a fast iterative solver in configuration space. To this end, we map the mean-field equations into configuration space with the expansion

$$\psi_\alpha = \sum_{n=1}^{\Omega} \varphi_n c_{n\alpha}, \quad (28)$$

where  $\{\varphi_n\}$  is a set of s.p. states acting as the expansion basis. For simplicity we choose an expansion basis such that  $c_{n\alpha}^{(0)} = \delta_{n\alpha}$  at the beginning. Inserting (28) into the HFB mean-field equations (11) yields

$$\lambda_{\beta\alpha}^- = \sum_{mn} c_{n\beta}^* \left\langle \varphi_n \left| \frac{\hat{\mathcal{H}}_\alpha - \hat{\mathcal{H}}_\beta}{2} \right| \varphi_m \right\rangle c_{m\alpha} = 0. \quad (29)$$

Eq. (29) is essentially the same as the symmetry condition (13a). It is solved by a simple damped gradient iteration:

$$\begin{aligned} c_{n\alpha}^{(\text{new})} &= \hat{O} \left\{ c_{n\alpha} - \frac{\delta}{h_{nn} - h_{11} + E_0} \left[ \sum_m \mathcal{H}_{\alpha, nm} c_{m\alpha} - \sum_{\beta} c_{n\beta} \lambda_{\beta\alpha} \right] \right\} \\ &= \hat{O} \left\{ c_{n\alpha} - \frac{\delta}{h_{nn} - h_{11} + E_0} \sum_{\beta} c_{n\beta} \lambda_{\beta\alpha} \right\}, \end{aligned} \quad (30)$$

where  $\mathcal{H}_{\alpha, nm} = \langle \varphi_n | \hat{\mathcal{H}}_{\alpha} | \varphi_m \rangle$  and

$$\lambda_{\beta\alpha} = \frac{1}{2} \sum_{mn} c_{n\beta}^* (\mathcal{H}_{\alpha, nm} + \mathcal{H}_{\beta, nm}) c_{m\alpha}. \quad (31)$$

The (interlaced) solution of the gap equations remains as before, but we do not update the local densities, the HF Hamiltonian  $\hat{h}$  and the pairing potential  $\hat{\bar{h}}$  in configuration space. The convergence of the iteration is checked, again, by the symmetry conditions (13b). The most efficient combination of the full 3D step with the iterations in configuration space is a matter of experience, see Sec. 4.

### 3.4. Soft cutoff on pairing-active space

It is well known that the HFB equations with local interactions diverge when solved in infinite quasiparticle/canonical space [1]. To limit the pairing-active space, all local densities (3) are augmented by the cutoff factor  $w_{\alpha}$ , for instance the particle and pairing densities:

$$\rho(\mathbf{r}) = \sum_{\alpha} w_{\alpha} v_{\alpha}^2 \sum_s |\psi_{\alpha}(\mathbf{r}, s)|^2, \quad (32a)$$

$$\xi(\mathbf{r}) = \sum_{\alpha} w_{\alpha} u_{\alpha} v_{\alpha} \sum_s |\psi_{\alpha}(\mathbf{r}, s)|^2. \quad (32b)$$

The same augment also applies to the kinetic-energy and the spin-orbit densities. A fixed number of states (realized by setting  $w_{\alpha} = 1$  or 0) is dangerous for two reasons. First, it hinders the portability of the pairing functional between codes and nuclei, because the s.p. space depends on the basis representation. Second, level crossings near the hard cutoff can induce jumps of the pairing energy. These problems can be solved by pairing renormalization [3, 46] which, however, could be impractical in a full 3D treatment that involves huge canonical spaces. Therefore, a commonly used remedy is to use a soft pairing cutoff [47, 48]

$$w_{\alpha} = \frac{1}{1 + \exp\left(\frac{h_{\alpha\alpha} - \epsilon_F - \Delta\epsilon_{\text{cut}}}{\Delta\epsilon_{\text{cut}}/10}\right)}. \quad (32c)$$

The cutoff places a fixed band  $\Delta\epsilon_{\text{cut}}$  above the actual Fermi energy  $\epsilon_F$ . We are going to use here  $\Delta\epsilon_{\text{cut}} = 15$  MeV. It is important to note that the soft cutoff modifies the state-dependent Hamiltonian  $\hat{\mathcal{H}}_{\alpha}$ :

$$\hat{\mathcal{H}}_{\alpha} = w_{\alpha} \left( v_{\alpha}^2 \hat{h} + u_{\alpha} v_{\alpha} \hat{\bar{h}} \right), \quad (33)$$

which defines all the ingredients entering the canonical HFB equations.

### 3.5. Strategies to avoid premature pairing breakdown

The pairing comes along with a second-order superfluid-to-normal phase transition. Below the critical pairing strength, the HFB pairing gap remains exactly zero. Above this critical strength, pairing becomes active and the gap starts to grow quickly. However, the onset of pairing is often delayed in a numerical calculation. The problem is that zero pairing remains a valid solution to the HFB (BCS) equations, but an unstable one. It can then take a very long time before the algorithm overcomes the instability and drives towards a stable solution. As a consequence, an iteration scheme can easily be deadlocked due to a pairing breakdown. This is a well-known problem. Most algorithms incorporate recovery strategies, such as occasional kick-offs by giving the pairing gap an artificial value, small enough not to spoil the physics but large enough to revive the pairing mechanism.

There is a more insidious problem with the state-dependent pairing gap  $\Delta_{\alpha\alpha}$ : It can happen that one canonical state logs out from the pairing scenario and gets stuck in its own pairing breakdown  $\Delta_{\alpha\alpha} \rightarrow 0$ . To understand that, we inspect Eq. (11) and recall that  $\hat{\mathcal{H}}_{\alpha} = v_{\alpha} \left( v_{\alpha} \hat{h} + u_{\alpha} \hat{\bar{h}} \right)$ . Far above the Fermi energy, we encounter states with  $u_{\alpha} \gg v_{\alpha}$  such that  $\hat{\mathcal{H}}_{\alpha} \approx \hat{\bar{h}}$  becomes a purely local operator. The solution to the mean field equation is  $\psi \propto \delta(\mathbf{r} - \mathbf{r}_{\text{min}})$  where  $\mathbf{r}_{\text{min}}$  is the point  $\hat{\bar{h}}$  has a minimum. In practice, this will be the representative of a  $\delta$ -function on the grid, slightly mellowed by orthonormalization to other states. As a consequence, the state acquires a very high kinetic energy and a very high canonical s.p. energy, which drives the solution of the gap equation (19) even more toward  $v_{\alpha} \rightarrow 0$ . This as such is a valid physical mechanism as long as the iterations curb down the occupations slowly from above. It becomes a problem if some  $v_{\alpha}$  gets stuck at zero at the very early stage of the iterative process. Once this has happened, the state  $\alpha$  is locked out of the pairing space. In order to avoid this from happening, we adopt a strategy similar to simulated annealing [49] and start the iteration scheme with an enhanced effective pairing strength which gradually reduces to the physical strength as

$$V_{\text{pair}}^{(\text{eff})} = V_{\text{pair}} \left( \eta_{\text{enh}} \frac{\max(\mathcal{N}_{\text{enh}} - \text{iter}, 0)}{\mathcal{N}_{\text{enh}}} + 1 \right), \quad (34)$$

where  $\text{iter}$  is the iteration number. In practice, we use an enhancement factor  $\eta_{\text{enh}} = 2$  and  $\mathcal{N}_{\text{enh}} = 400$ . With this choice, the lock-in problem in the most critical early phases of iterations is avoided.

### 3.6. Hermiticity restoration

According to Refs. [21, 22], the explicit expression of applying the Skyrme HF Hamiltonian  $\hat{h}$  on a wave function  $\psi$  can be written as:

$$\begin{aligned} \hat{h}\psi &= U(\mathbf{r})\psi - \nabla \cdot [B(\mathbf{r})\nabla]\psi \\ &\quad + \frac{i}{2} [\mathbf{W} \cdot (\boldsymbol{\sigma} \times \nabla)\psi + \boldsymbol{\sigma} \cdot \nabla \times (\mathbf{W}\psi)]. \end{aligned} \quad (35)$$

This expression can be directly derived from the Skyrme EDF via Eq. (6), without invoking the product rule. In [22] it was noted that the product rule is not perfectly fulfilled when derivatives are evaluated via the discrete Fourier transform. Therefore, in SKY3D version 1.1 the commonly-adopted form of the spin-orbit term

$$i\mathbf{W} \cdot (\boldsymbol{\sigma} \times \nabla)\psi \quad (36)$$

was replaced by the one given in Eq. (35); with  $\nabla \times \mathbf{W} = 0$ , these two forms are connected by the product rule. However, the second term of  $\hat{h}\psi$ , which involves a position-varying differential operator, is still calculated through the product rule in SKY3D:

$$\nabla \cdot [B(\mathbf{r})\nabla]\psi = \sum_{i=x,y,z} \frac{\partial B}{\partial i} \frac{\partial \psi}{\partial i} + B \frac{\partial^2 \psi}{\partial i^2}. \quad (37)$$

Unfortunately, evaluating Eq. (37) with the FFT-based differentiation breaks the Hermiticity of the operator [50]. This point is confirmed by computed results shown in Sec. 4.3.

Instead of using Eq. (37), the simplest way to restore Hermiticity in the evaluation of  $\nabla \cdot (B\nabla\psi)$  is to compute two consecutive first-order derivatives. But, as discussed in Sec. 3.1, this creates a problem with the second derivative that involves the Fourier component  $\tilde{\psi}(k_{N_x/2+1})$ . According to Ref. [50], one should keep the term  $\tilde{\psi}(k_{N_x/2+1})$  in the two first derivatives, and average the results of  $k_{N_x/2+1} = \pm \frac{N_x}{2} \delta k$  to maintain the symmetry in Fourier space. One can show that this “average” algorithm is equivalent to Algorithm 1 (Algorithm 3 in [50]), which is simpler to compute and thus implemented in HFBFFT. In Algorithm 1, one first computes an FFT-based first derivative, with  $\tilde{\psi}(k_{N_x/2+1})$  saved and then zeroed before the inverse FFT is performed on  $ik_n \tilde{\psi}(k_n)$  (steps 1 through 3). Then one multiplies in coordinate space with the field  $B(x)$  involved (step 4). Finally, one computes the derivative of the  $B\psi'$  thus obtained with modifying  $\tilde{\phi}(k_{N_x/2+1})$  so that we can keep Hermiticity without losing the information of  $\tilde{\psi}(k_{N_x/2+1})$  (steps 5 through 7). The position-varying differential operator also appears in many other physics equations, like the heat equation with varying diffusivity and Poisson’s equation with changing permittivity; hence, Algorithm 1 has a broad application range.

---

**Algorithm 1** Compute the one-dimensional position-varying differentiation  $\frac{d}{dx} [B(x) \frac{d\psi}{dx}]$ .

---

- 1: Compute Fourier transform  $\tilde{\psi}_n = \text{FFT}[\psi_v]$  with  $\psi_v = \psi(x_v)$ .
  - 2: Save  $\tilde{\psi}_{N_x/2+1} \rightarrow \tilde{\Psi}$ , build  $\tilde{\psi}'_n = ik_n \tilde{\psi}_n$  with  $\tilde{\psi}'_{N_x/2+1} = 0$ .
  - 3: Compute inverse transform  $\psi'_v = \text{FFT}^{-1}[\tilde{\psi}'_n]$ .
  - 4: Build  $\phi_v = B_v \psi'_v$  with  $B_v = B(x_v)$ .
  - 5: Compute Fourier transform  $\tilde{\phi}_n = \text{FFT}[\phi_v]$ .
  - 6: Build  $\tilde{\phi}'_n = ik_n \tilde{\phi}_n$  and set  $\tilde{\phi}'_{N_x/2+1} = -\frac{\sum_{v=1}^{N_x} c_v}{N_x} \left(\frac{N_x}{2} \delta k\right)^2 \tilde{\Psi}$ .
  - 7: Compute inverse transform  $\frac{d}{dx} [B(x) \frac{d\psi}{dx}]_v = \text{FFT}^{-1}[\tilde{\phi}'_n]$ .
- 

### 3.7. Numerical realization in harmonic-oscillator basis

The HFB solutions obtained with the HFBFFT code will be compared with the well-established code HFBTHO. This code has been extensively documented in several publications [12, 13]. The solver HFBTHO uses an expansion of the s.p. wave functions in the basis of axially symmetric HO (or transformed HO) states. The basis is given by the number of oscillator shells that defines the s.p. space size, as well as the oscillator length and deformation that determine the HO wave functions. Local fields in HFBTHO are handled on the Gaussian integration points and the Gaussian integration rule is used to compute integrals.

A major difference between the two codes lies in the way the HFB equations are solved. HFBFFT uses a representation in terms of the canonical basis, see Sec. 3, while HFBTHO works in a quasiparticle space. The results are fully equivalent if the same number of s.p. states is used. Differences appear in connection with the cutoff in pairing space. HFBFFT defines the cutoff in terms of the canonical s.p. energies, whereas HFBTHO does that in terms of the quasiparticle energies. This, taken together with the fact that the pairing strength has to depend on the size of the pairing space, means that the values of  $V_{\text{pair},q}$  are not fully portable. It will play a role in the benchmarking tests presented in Sec. 4.

## 4. Benchmarks

In this section, we benchmark HFBFFT against HFBTHO, SKY1D, and SKY2D. These codes have symmetry restrictions. SKY1D enforces spherical symmetry and can be used for magic nuclei. HFBTHO and SKY2D allow for axially symmetric shapes and cover all test cases here. Those codes can run with or without imposing reflection symmetry.

First, we determine appropriate parameters to use, including the box size and grid spacing. Before making comparisons with other solvers, we quantify the effect brought by the Hermiticity restoration. In the next step, we compare some characteristic nuclei ranging from spherical doubly magic  $^{132}\text{Sn}$  and  $^{208}\text{Pb}$ , to spherical superfluid  $^{120}\text{Sn}$ , to deformed superfluid  $^{102,110}\text{Zr}$ , to superdeformed fission isomer in  $^{240}\text{Pu}$ . In all these calculations, we use the Skyrme functional SLy4 [51] in the particle-hole channel and the mixed density-dependent  $\delta$  interaction ( $\rho_{0,\text{pair}} = 0.32 \text{ fm}^{-3}$  in Eq. (4d)) in the particle-particle channel.

### 4.1. Parameter determination

To ensure the correct asymptotic behavior near the box boundary, we use  $^{110}\text{Zr}$  to determine the appropriate box and grid sizes. The nucleus  $^{110}\text{Zr}$  is chosen because it has a significant neutron excess and thus weakly bound canonical states. The calculated proton and neutron densities were inspected for different box lengths and different grids. Based on this analysis, we adopted a cubic box with a side length of 37.6 fm and 48 grid points in each dimension (spacing between two neighboring points is 0.8 fm). With the above settings, the proton and neutron densities are below  $10^{-7}$  nucleons/fm<sup>3</sup> at the boundary,

which is small enough for our tests. For spherical nuclei such as  $^{120}\text{Sn}$ , a smaller box is usually sufficient.

We take 176 neutron and 126 proton canonical states ( $\Omega_n = 176$ ,  $\Omega_p = 126$ ), 15 MeV energy cutoff for the pairing window. This number of active states is determined by the tests for spherical  $^{120}\text{Sn}$  and deformed  $^{110}\text{Zr}$  nuclei. When we increase the number of active states to 200 neutron and 150 proton states, the total energy remains stable within 10 keV. In order to speed up the convergence, we perform 100 sub-iteration steps in the configuration space between two gradient iterations in the coordinate space, initialize with 30 HF+BCS steps, and employ the pairing enhancement factors defined in Sec. 3.5.

For HFBTHO calculations, we take 25 HO shells for both protons and neutrons unless explicitly stated otherwise. An axially deformed HO basis with  $\beta_2 = 0.2$  is used in deformed nuclei ground state calculations ( $^{102,110}\text{Zr}$  and  $^{240}\text{Pu}$ ) and  $\beta_2 = 0.6$  is used to calculate the  $^{240}\text{Pu}$  fission isomer. For the spherical nuclei, we also compare HFBFFT with the results of the 1D spherical HFB code SKY1D, which uses a radial coordinate-space mesh and the five-point finite difference formula for derivatives. The mesh spacing and the number of points we employ in SKY1D are 0.15 fm and 141, respectively. For the deformed nuclei, we compare HFBFFT results with the 2D axial HFB code SKY2D, which uses 31 points in both  $r$ - and  $z$ -directions with a mesh spacing of 0.7 fm. Since the nuclei considered in this study are all reflection-symmetric, the grid extends from  $z = 0$  fm to  $z = 21$  fm.

#### 4.2. Pairing renormalization

As we mentioned in Sec. 3.7, pairing strengths are not portable between HFBFFT and HFBTHO because of different descriptions of the pairing space and different structures of one-quasiparticle continuum in these two solvers. Therefore, we need to renormalize the pairing strengths to compare results for open-shell nuclei in which pairing is essential. Intuitively, there are several choices for pairing renormalization.

For instance, one can tune pairing strengths to reproduce the pairing energies in different solvers. However, as discussed in [52, 46], the pairing energy density is divergent with respect to the cutoff energy. A better measure is the quantity

$$\tilde{E}_{\text{kin}}^q = E_{\text{kin}}^q + E_{\text{pair}}^q \quad (q = n \text{ or } p), \quad (38)$$

which is less sensitive to the pairing cutoff energy. As it will be shown in Sec. 4.4, the kinetic energy strongly depends on the basis size in HFBTHO. Therefore, in situations when the error related to the choice of the basis, or spatial grid, dominates,  $\tilde{E}_{\text{kin}}$  will be a poor renormalization measure. Another pairing measure is the spectral pairing gap [1, 3, 53]

$$\Delta^q \equiv \frac{\sum_{\alpha \in q} w_{\alpha} v_{\alpha}^2 \Delta_{\alpha}}{\sum_{\alpha \in q} w_{\alpha} v_{\alpha}^2} \quad (q = n \text{ or } p). \quad (39)$$

This quantity has been used in numerous papers to adjust pairing strengths to observed odd-even mass differences and we shall use it in this study to renormalize the pairing channel of different solvers.

#### 4.3. Energy shift by Hermiticity restoration

As we mentioned in Sec. 3.6, the product rule in the FFT-based differentiation violates the Hermiticity of the position-varying differential operator. To restore the Hermiticity, we implement Algorithm 1 in HFBFFT. The results are shown in Table 1 for several nuclei. The Hermiticity violation is demonstrated by a non-vanishing  $\Delta S^2 \sim 10^{-6} \text{ MeV}^2$  in the calculations of spherical nuclei  $^{132}\text{Sn}$  and  $^{208}\text{Pb}$  for which the static pairing vanishes and hence the HFB calculation is reduced to HF. As for other open-shell nuclei with non-vanishing pairing, their  $\Delta S^2$  values are similar before and after the Hermiticity restoration. These values of  $\Delta S^2$  are characteristic of the accuracy typically achieved in HFBFFT and they are larger than the error due to the Hermiticity breaking. In terms of the total energy, the effect is of the order of a few keV, i.e., insignificant for many practical applications. Even so, Hermiticity breaking effects can affect some calculations if not remedied. For example, the small error brought by the Hermiticity breaking can accumulate step by step in a time-dependent calculation.

HFBFFT	Hermiticity broken		Hermiticity restored	
	$E_{\text{tot}}$	$\Delta S^2$	$E_{\text{tot}}$	$\Delta S^2$
$^{132}\text{Sn}$	-1103.5429	3.91E-06	-1103.5423	4.15E-14
$^{208}\text{Pb}$	-1635.6817	6.61E-06	-1635.6807	6.40E-14
$^{120}\text{Sn}$	-1018.3310	3.11E-05	-1018.3305	3.45E-05
$^{110}\text{Zr}$	-893.8578	3.09E-05	-893.8574	4.02E-05
$^{102}\text{Zr}$	-859.4696	3.00E-05	-859.4692	2.19E-05

Table 1: Total energies  $E_{\text{tot}}$  (in MeV) and  $\Delta S^2$  (in  $\text{MeV}^2$ ) for five nuclei calculated with HFBFFT without and with the Hermiticity restoration. The digits which do not coincide before and after the Hermiticity restoration are marked in bold.

#### 4.4. Doubly magic nuclei: $^{132}\text{Sn}$ and $^{208}\text{Pb}$

In the first step, we calculate two doubly magic unpaired nuclei  $^{132}\text{Sn}$  and  $^{208}\text{Pb}$ . For these nuclei, the results of HFBFFT and SKY3D are identical. In Table 2, we list the ground-state energies as well as contributions from various functional terms, obtained from four solvers HFBFFT, HFBTHO, SKY1D and SKY2D for  $^{132}\text{Sn}$ . Table 3 shows similar results for  $^{208}\text{Pb}$ . When

$^{132}\text{Sn}$	HFBTHO	HFBFFT	SKY1D	SKY2D
$E_{\text{tot}}$	-1103.49	-1103.54	-1103.57	-1103.56
$E_{\text{kin}}^n$	1637.71	1637.97	1638.01	1638.02
$E_{\text{kin}}^p$	808.44	808.57	808.59	808.56
$E_{\rho\rho}$	-4876.26	-4877.02	-4877.04	-4877.07
$E_{\rho\tau}$	821.49	821.70	821.73	821.72
$E_{\rho\Delta\rho}$	248.11	248.23	248.25	248.23
$E_{\rho\nabla J}$	-84.40	-84.43	-84.44	-84.43
$E_{\text{Coul}}$	341.42	341.44	341.44	341.43

Table 2: Energy contributions (in MeV) to the binding energy of for  $^{132}\text{Sn}$  computed with HFBTHO, HFBFFT, SKY1D, and SKY2D. The digits which do not coincide with HFBFFT are marked in bold.

we compare HFBFFT with SKY1D and SKY2D for  $^{132}\text{Sn}$ , we



find the energy differences do not usually exceed 40 keV. Such small differences can be traced back to different box boundary conditions assumed in these codes. In HFBFFT, calculations are performed in a 3D rectangular box while the box is represented by a spherical shell in SKY1D and a cylindrical shape in SKY2D. For a well-bound nucleus and large spatial boxes, the results should be practically independent of the geometry of the box. As seen in Table 2 this indeed holds for  $^{132}\text{Sn}$ . As we will see below, larger box-related errors are expected in superfluid and/or weakly bound nuclei. For nuclear matter and time-dependent calculations, the finite-size box errors can be appreciable; they can be greatly reduced by imposing twist-averaged boundary conditions [54].

We find about 50 keV energy difference between HFBTHO and HFBFFT; this difference can be primarily traced back to  $E_{\text{kin}}$  and  $E_{\rho\rho}$ . As discussed in Refs. [55, 56], the kinetic energy converges slowly in the HO basis. To investigate this effect, we calculate  $^{208}\text{Pb}$  using different numbers of HO shells in HFBTHO. We see in Table 3 that when we increase the number of HO shells to 30, the HFBTHO energies approach the HFBFFT values. It is also seen that  $E_{\text{kin}}$  and  $E_{\rho\rho}$  exhibit the largest variations with  $N$ .

In Refs. [55, 57], the correction to the ground-state energy due to the finite number of HO shells  $N$  has been derived:

$$E_L = E_\infty + a_0 e^{-2k_\infty L}, \quad (40)$$

where  $L \equiv \sqrt{2(N + 3/2 + 2)}b$ ,  $b$  is the oscillator length of our HO basis, and  $a_0$ ,  $k_\infty$  and  $E_\infty$  are fit parameters. Then  $E_\infty$  is the energy in the limit of infinitely large model space. The fit of  $E_{\text{tot}}$  to Eq. (40) is presented in Fig. 1 and the resulting value of  $E_\infty = -1635.786$  MeV agrees fairly well with the HFBFFT and SKY1D values. Hence, obtaining an accurate kinetic as well as total energies in a HO basis-expansion solver requires a huge number of shells. In this context, the use of the coordinate-space representation is beneficial.

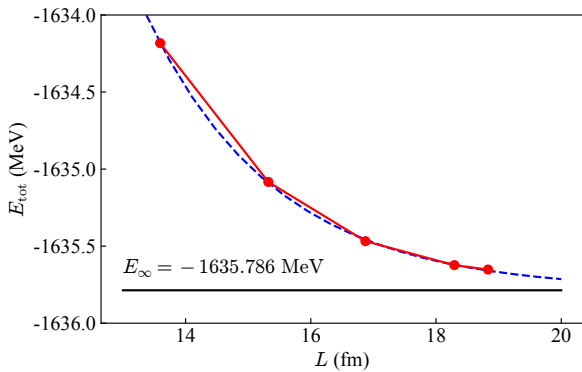


Figure 1:  $E_{\text{tot}}$  as a function of  $L$  for  $^{208}\text{Pb}$ . The HFBTHO results are marked by red dots. The blue curve is fitted according to Eq. (40).

#### 4.5. Spherical superfluid nucleus: $^{120}\text{Sn}$

We now calculate  $^{120}\text{Sn}$  which has a non-vanishing neutron pairing. The neutron pairing strength  $V_{\text{pair},n}$  in HFBTHO

is adjusted to the average experimental neutron pairing gap  $\Delta_n = 1.25$  MeV. In HFBFFT, SKY1D and SKY2D, two pairing renormalizations are used. In the first variant, the neutron pairing strengths are adjusted to reproduce the HFBTHO value of  $\tilde{E}_{\text{kin}}^n$ . In the second variant, the HFBTHO value of  $\Delta^n$  is matched. The results for both variants are displayed in Table 4. The neutron pairing strengths vary between the solvers, reflecting different structures of their quasiparticle pairing spaces, i.e., different pairing cutoff procedures and different structures of the discretized one-quasiparticle continuum.

Although there are large discrepancies in  $E_{\text{kin}}^n$  and  $E_{\text{pair}}^n$  between HFBFFT and HFBTHO, in the first renormalization variant, the difference of the total energy, about 0.4 MeV, is quite reasonable considering the fact that the pairing space is treated differently and the HFBTHO results are affected by the basis truncation error. The difference in  $E_{\text{tot}}$  between the three coordinate-space solvers, less than 150 keV, reflects the dependence of the level density of the discretized quasiparticle continuum on the box boundary conditions assumed.

In the pairing gap renormalization variant, the agreement of  $E_{\text{tot}}$  is even better, with only 10-30 keV difference between HFBFFT, HFBTHO and SKY2D. In this variant, the magnitudes of the neutron pairing energy and kinetic energy are considerably larger as compared to the variant in which  $\tilde{E}_{\text{kin}}^n$  is renormalized. Still, as seen in Table 4, both pairing renormalizations work reasonably well for  $^{120}\text{Sn}$ . It is interesting to note that the total root-mean-square (rms) radii  $r_{\text{rms}}$  are predicted very robustly in all renormalization variants.

#### 4.6. Axially deformed nuclei: $^{102,110}\text{Zr}$

The neutron-rich nuclei  $^{102,110}\text{Zr}$  are suitable test cases, as they are known/expected to have large prolate deformations. In addition,  $^{110}\text{Zr}$  is weakly bound, with the neutron chemical potential  $\epsilon_{F,n} \approx -3.5$  MeV. The HFB proton pairing vanishes in this nucleus. In Table 5, we show results for  $^{110}\text{Zr}$  with the two pairing renormalization schemes investigated in Sec. 4.5. It is seen that the HFBFFT results for various observables, i.e., total energy, quadrupole moments, and the rms radii, all agree well with those from HFBTHO in both pairing variants.

In the case of  $^{102}\text{Zr}$ , one also needs to consider proton pairing. In this case, we renormalize both neutron and proton spectral pairing gaps by reproducing their values obtained from HFBTHO. In the calculation, 25 HO shells for both neutrons and protons are employed in HFBTHO, which means that the s.p. proton and neutron spaces are the same. In HFBFFT, the canonical spaces are different as  $\Omega_n = 176$ ,  $\Omega_p = 126$ . However, the actual pairing space is set by the soft-cutoff factor  $w_\alpha$ . It is seen in Table 6 that the benchmarking results following the pairing renormalization are very satisfactory. In particular, the results of HFBFFT, HFBTHO, and SKY2D are fairly close for the observables:  $E_{\text{tot}}$ ,  $r_{\text{rms}}$ , and quadrupole moments.

#### 4.7. Superdeformed heavy nucleus: $^{240}\text{Pu}$

Compared with the HO basis, the coordinate-space representation can better capture strongly deformed configurations, such as the superdeformed fission isomer (f.i.) in  $^{240}\text{Pu}$ . Indeed,

$^{208}\text{Pb}$	$N=15$	$N=20$	$N=25$	$N=30$	HFBFFT	SKY1D
$E_{\text{tot}}$	-1634. <b>25</b>	-1635. <b>16</b>	-1635. <b>46</b>	-1635. <b>62</b>	-1635.68	-1635.70
$E_{\text{kin}}^n$	2525. <b>13</b>	2527. <b>80</b>	2528. <b>42</b>	2528. <b>83</b>	2529.13	2529.16
$E_{\text{kin}}^p$	1334. <b>56</b>	1336. <b>34</b>	1336. <b>71</b>	1336. <b>91</b>	1337.06	1337.07
$E_{\rho\rho}$	-7835. <b>80</b>	-7844. <b>07</b>	-7845. <b>66</b>	-7846. <b>67</b>	-7847.54	-7847.63
$E_{\rho\tau}$	1327. <b>84</b>	1329. <b>55</b>	1329. <b>79</b>	1329. <b>98</b>	1330.20	1330.22
$E_{\rho\Delta\rho}$	314. <b>05</b>	315. <b>12</b>	315. <b>12</b>	315. <b>17</b>	315.29	315.29
$E_{\rho\nabla J}$	-96. <b>30</b>	-96. <b>44</b>	-96. <b>42</b>	-96. <b>43</b>	-96.45	-96.45
$E_{\text{Coul}}$	796. <b>26</b>	796. <b>55</b>	796. <b>56</b>	796. <b>60</b>	796.63	796.63

Table 3: Energies for  $^{208}\text{Pb}$  from HFBTHO (computed with different number of HO shells  $N$ ), HFBFFT, and SKY1D. All energies are in MeV. The digits which do not coincide with HFBFFT are marked in bold.

$^{120}\text{Sn}$	HFBTHO	HFBFFT	SKY1D $\tilde{E}_{\text{kin}}^n$ -renorm.	SKY2D	HFBFFT	SKY1D $\Delta^n$ -renorm.	SKY2D
$E_{\text{tot}}$	-1018. <b>77</b>	-1018.34	-1018. <b>45</b>	-1018.37	-1018.78	-1018. <b>92</b>	-1018.74
$E_{\text{Coul}}$	347. <b>37</b>	347.44	347. <b>45</b>	347.41	347.47	347. <b>49</b>	347.45
$E_{\text{kin}}^n$	1340. <b>51</b>	1335.40	1335. <b>18</b>	1335.43	1339.17	1339.14	1338. <b>72</b>
$E_{\text{kin}}^p$	830. <b>75</b>	830.97	831. <b>01</b>	830.01	831.25	831.31	831.28
$E_{\text{pair}}^n$	-12. <b>48</b>	-7.37	-7. <b>15</b>	-7.40	-9.29	-9.14	-9. <b>02</b>
$\tilde{E}_{\text{kin}}^n$	1328.03	1328.03	1328.03	1328.03	1329.88	1330.01	1329.70
$\Delta^n$	1.25	1.08	1.07	1.09	1.25	1.25	1.25
$\epsilon_{\text{F},n}$	-8.02	-8.01	-8.01	-8.04	-8.00	-8.00	-8.04
$V_{\text{pair},n}$	-284.57	-342.70	-346.50	-354.90	-361.80	-367.30	-372.35
$r_{\text{rms}}$	4.67	4.67	4.67	4.67	4.67	4.67	4.67

Table 4: Results of HFB + SLy4 calculations for  $^{120}\text{Sn}$  using HFBTHO, HFBFFT, SKY1D, and SKY2D. Two neutron pairing renormalization variants are considered, by adjusting the neutron pairing strengths in HFBFFT, SKY1D, and SKY2D to reproduce the HFBTHO values of  $\tilde{E}_{\text{kin}}^n$  and  $\Delta^n$ . All energies are in MeV. The radius  $r_{\text{rms}}$  is in fm. The digits which do not coincide with HFBFFT are marked in bold.

very large configuration spaces are needed to guarantee the convergence of the HO expansion at large deformations [58, 59]. Given the large number of nucleons in  $^{240}\text{Pu}$ , one needs to carefully consider the number of canonical states in HFBFFT and SKY2D calculations. To this end, we performed a series of calculations by increasing the canonical space until the convergence had been reached. This has been done separately for the ground state (g.s.) and f.i. of  $^{240}\text{Pu}$ . The final values are:  $(\Omega_n, \Omega_p) = (300, 200)$  for the g.s. and  $(\Omega_n, \Omega_p) = (400, 300)$  for the f.i. calculations. We renormalize the pairing strengths for  $^{240}\text{Pu}$  to reproduce the g.s.  $\Delta^n$  and  $\Delta^p$  obtained in HFBTHO. The results are displayed in Table 7.

In HFBTHO and SKY2D, the f.i. is found by performing quadrupole-moment constrained calculations. The f.i. configuration in HFBFFT was computed by initializing the code with various HO deformations. As seen in Table 7, HFBTHO and HFBFFT results are very similar for g.s. energies, g.s. quadrupole deformations, and radii.

To test the functionality of HFBFFT for the f.i., we renormalize pairing strengths in HFBFFT and SKY2D to the HFBTHO pairing gaps. Both coordinate-space solvers give very close results for the f.i., and they agree nicely with the HFBTHO results, see Table 7. Overall, the  $^{240}\text{Pu}$  results obtained with HFBFFT for both the g.s. and f.i. show reasonable agreement with those from HFBTHO.

## 5. Conclusions

We developed a 3D Skyrme HFB solver HFBFFT in the coordinate-space representation using the canonical basis approach. The code is based on the well-optimized SKY3D solver. In HFBFFT we implemented several new elements to facilitate calculations, namely (i) the sub-iteration method in configuration space to accelerate the convergence; (ii) the soft pairing cutoff and pairing annealing to avoid pairing breakdown; and (iii) a new algorithm to restore the Hermiticity of the HFB matrix.

The new solver has been benchmarked for several spherical and deformed nuclei against HFBTHO, SKY2D, and (for spherical systems) SKY1D. The representation of the positive-energy continuum differs between HFB codes: In particular, it depends on the code's geometry (spherical, cylindrical, Cartesian), the size of s.p. configuration space (number of HO shells, box size, grid size), and the effective pairing space. Consequently, even if the EDFs employed in two codes are identical, the pairing channel is usually described differently. This creates problems when comparing different HFB solvers as the perfect benchmarking is practically impossible [19]. In this work, we carried our inter-code comparisons by renormalizing pairing strengths to the spectral pairing gaps and/or the effective kinetic energy  $\tilde{E}_{\text{kin}}$ . While both methods give similar results, spectral pairing gaps are less sensitive to the s.p. space assumed.

$^{110}\text{Zr}$	HFBTHO	HFBFFT	Sky2D	HFBFFT	Sky2D
		$\tilde{E}_{\text{kin}}^n$ -renorm.		$\Delta^n$ -renorm.	
$E_{\text{tot}}$	-893. <b>97</b>	-894. <b>33</b>	-894. <b>32</b>	-894. <b>01</b>	-894. <b>01</b>
$E_{\text{Coul}}$	226. <b>72</b>	226. <b>72</b>	226. <b>71</b>	226. <b>74</b>	226. <b>70</b>
$E_{\text{kin}}^n$	1368. <b>08</b>	1369. <b>22</b>	1368. <b>98</b>	1367. <b>86</b>	1367. <b>13</b>
$E_{\text{kin}}^p$	632. <b>03</b>	632. <b>05</b>	632. <b>13</b>	632. <b>16</b>	632. <b>05</b>
$E_{\text{pair}}^n$	-3. <b>18</b>	-4. <b>31</b>	-4. <b>08</b>	-2. <b>30</b>	-2. <b>19</b>
$\tilde{E}_{\text{kin}}^n$	1364.90	1364.90	1364.90	1365.56	1364.94
$\Delta^n$	0.64	0.93	0.92	0.64	0.64
$\epsilon_{F,n}$	-3.55	-3.50	-3.52	-3.55	-3.57
$V_{\text{pair},n}$	-284.57	-409.80	-428.00	-371.00	-384.80
$r_{\text{rms}}$	4.73	4.73	4.74	4.73	4.74
$Q_{20}^n$	789	794	795	791	796
$Q_{20}^p$	444	447	447	445	447

Table 5: Results of HFB + SLy4 calculations for  $^{110}\text{Zr}$  with HFBTHO, HFBFFT and Sky2D. Two neutron pairing renormalization variants are considered, by adjusting the neutron pairing strengths in HFBFFT and Sky2D to reproduce the HFBTHO values of  $\tilde{E}_{\text{kin}}^n$  and  $\Delta^n$ . All energies are in MeV. The radius  $r_{\text{rms}}$  is in fm and quadrupole moments  $Q_{20}^{p,n}$  are in fm<sup>2</sup>. The HFB proton pairing vanishes in this nucleus. The digits which do not coincide with HFBFFT are marked in bold.

$^{102}\text{Zr}$	HFBTHO	HFBFFT	Sky2D
$E_{\text{tot}}$	-859. <b>65</b>	-859. <b>69</b>	-859.67
$E_{\text{Coul}}$	231.11	231.16	231.14
$E_{\text{kin}}^n$	1202. <b>02</b>	1200. <b>96</b>	1201. <b>97</b>
$E_{\text{kin}}^p$	651.25	651.22	651.27
$E_{\text{pair}}^n$	-3. <b>39</b>	-2. <b>50</b>	-2. <b>39</b>
$E_{\text{pair}}^p$	-1. <b>97</b>	-1.42	-1.38
$\tilde{E}_{\text{kin}}^n$	1198. <b>63</b>	1199.53	1199.58
$\tilde{E}_{\text{kin}}^p$	649. <b>28</b>	649.79	649.89
$\Delta^n$	0.69	0.69	0.69
$\Delta^p$	0.56	0.56	0.56
$\epsilon_{F,n}$	-5.43	-5.42	-5.44
$\epsilon_{F,p}$	-12.09	-12.09	-12.10
$V_{\text{pair}}^n$	-284.57	-367.00	-378.40
$V_{\text{pair}}^p$	-284.57	-372.00	-384.70
$r_{\text{rms}}$	4.58	4.58	4.58
$Q_{20}^n$	639	639	640
$Q_{20}^p$	411	411	411

Table 6: Results of HFB + SLy4 calculations for  $^{102}\text{Zr}$  using HFBTHO, HFBFFT and Sky2D. The pairing renormalization is carried out by adjusting the proton and neutron pairing strengths in HFBFFT and Sky2D to reproduce the HFBTHO values of  $\Delta^n$  and  $\Delta^p$ . All energies are in MeV. The radius  $r_{\text{rms}}$  is in fm and quadrupole moments  $Q_{20}^{p,n}$  are in fm<sup>2</sup>. The digits which do not coincide with HFBFFT are marked in bold.

By carrying out calculations with different HFB solvers, we were able to assess the ranges of different uncertainties. For the total energy, the typical errors are: several keV due to the Hermiticity breaking; 10-80 keV due to different box boundary conditions assumed; 10-140 keV due to different quasiparticle continuum discretizations; and several hundred keV due to the basis truncation in HO basis-expansion solvers.

As a 3D solver, HFBFFT is the tool of choice to study deformed and weakly bound systems. To make this tool versatile, several enhancements are planned. Most importantly, we intend to implement pairing regularization [5, 46, 34] to get rid of the

dependence of pairing strengths on the cutoff energy. Another essential development is to be able to compute potential energy surfaces defined by means of constraining one-body operators. This will enable us to use HFBFFT in the calculations of large-amplitude nuclear collective motions such as fission or fusion, for which the solvers based on the basis-expansion approach require the use of excessively large configuration spaces. Finally, the performance of HFBFFT needs to be further optimized for modern supercomputer architectures.

## Acknowledgments

Comments from Kyle Godbey are gratefully appreciated. Computational resources were provided by the Institute for Cyber-Enabled Research at Michigan State University. This material is based upon work supported by the U.S. Department of Energy, Office of Science, Office of Nuclear Physics under award numbers DE-SC0013365 and DE-SC0018083 (NUCLEI SciDAC-4 collaboration).

## References

- [1] J. Dobaczewski, H. Flocard, and J. Treiner, “Hartree-Fock-Bogolyubov description of nuclei near the neutron-drip line,” *Nucl. Phys. A*, vol. 422, no. 1, pp. 103 – 139, 1984. [Online]. Available: <http://www.sciencedirect.com/science/article/pii/0375947484904330>
- [2] S. T. Belyaev, A. V. Smirnov, S. V. Tolokonnikov, and S. A. Fayans, “Pairing in nuclei in the coordinate representation,” *Sov. J. Nucl. Phys.*, vol. 45, p. 783, 1987.
- [3] J. Dobaczewski, W. Nazarewicz, T. R. Werner, J. F. Berger, C. R. Chinn, and J. Dechargé, “Mean-field description of ground-state properties of drip-line nuclei: Pairing and continuum effects,” *Phys. Rev. C*, vol. 53, pp. 2809–2840, Jun 1996. [Online]. Available: <https://link.aps.org/doi/10.1103/PhysRevC.53.2809>
- [4] J. Dobaczewski and W. Nazarewicz, “Hartree-Fock-Bogoliubov solution of the pairing Hamiltonian in finite nuclei,” in *50 Years of Nuclear BCS*, R. A. Broglia and V. Zelevinsky, Eds. World Scientific, 2013, p. 40. [Online]. Available: <https://doi.org/10.1142/8526>
- [5] A. Bulgac, “Local density approximation for systems with pairing correlations,” *Phys. Rev. C*, vol. 65, no. 5, p. 051305, 2002. [Online]. Available: <http://link.aps.org/abstract/PRC/v65/e051305>

<sup>240</sup> Pu	ground state		fission isomer		
	HFBTHO	HFBFFT	HFBTHO	HFBFFT	SKY2D
$E_{\text{tot}}$	-1802.11	-1802.43	-1797.00	-1797.35	-1797.35
$E_{\text{Coul}}$	989.61	956.98	957.02	956.96	956.90
$E_{\text{kin}}^{\text{n}}$	2938.92	2939.94	2922.56	2923.45	2923.43
$E_{\text{kin}}^{\text{b}}$	1520.95	1521.46	1525.25	1525.52	1525.33
$E_{\text{pair}}^{\text{n}}$	-3.11	-2.30	-3.52	-2.60	-2.48
$E_{\text{pair}}^{\text{b}}$	-1.54	-1.22	-2.85	-2.19	-2.07
$\tilde{E}_{\text{kin}}^{\text{n}}$	2935.81	2937.64	2919.03	2920.85	2920.55
$\tilde{E}_{\text{kin}}^{\text{b}}$	1519.40	1520.25	1522.39	1523.33	1523.25
$\Delta^{\text{n}}$	0.44	0.44	0.47	0.47	0.47
$\Delta^{\text{p}}$	0.33	0.33	0.46	0.46	0.46
$\epsilon_{\text{F,n}}$	-5.71	-5.70	-5.66	-5.65	-5.67
$\epsilon_{\text{F,p}}$	-5.69	-5.70	-5.76	-5.77	-5.79
$r_{\text{rms}}$	5.93	5.93	6.40	6.40	6.40
$Q_{20}^{\text{n}}$	1784	1782	5063	5072	5071
$Q_{20}^{\text{b}}$	1166	1165	3336	3344	3343
$V_{\text{pair}}^{\text{n}}$	-284.57	-360.00	-284.57	-369.00	-384.60
$V_{\text{pair}}^{\text{p}}$	-284.57	-355.00	-284.57	-360.00	-375.80
s.p. space	25 shells	(300, 200)	25 shells	(400, 300)	(400, 300)

Table 7: Results of HFB + SLy4 calculations for <sup>240</sup>Pu ground state and fission isomer using HFBTHO, HFBFFT and Sky2D. The pairing strengths in HFBFFT and Sky2D were adjusted to reproduce the spectral pairing gaps obtained in HFBTHO for the g.s. and f.i. separately. The s.p. space for HFBFFT is defined by means of ( $\Omega_n$ ,  $\Omega_p$ ). All energies are in MeV,  $r_{\text{rms}}$  is in fm, and  $Q_{20}^{\text{b,n}}$  are in fm<sup>2</sup>. The digits which do not coincide with HFBFFT are marked in bold.

- [6] M. Bender, P.-H. Heenen, and P.-G. Reinhard, “Self-consistent mean-field models for nuclear structure,” *Rev. Mod. Phys.*, vol. 75, pp. 121–180, Jan 2003. [Online]. Available: <https://link.aps.org/doi/10.1103/RevModPhys.75.121>
- [7] N. Schunck, Ed., *Energy Density Functional Methods for Atomic Nuclei*, ser. 2053-2563. IOP Publishing, 2019. [Online]. Available: <http://dx.doi.org/10.1088/2053-2563/aae0ed>
- [8] T. Skyrme, “The effective nuclear potential,” *Nucl. Phys.*, vol. 9, no. 4, pp. 615 – 634, 1958. [Online]. Available: <http://www.sciencedirect.com/science/article/pii/0029558258903456>
- [9] J. Erler, P. Klüpfel, and P.-G. Reinhard, “Self-consistent nuclear mean-field models: example Skyrme-Hartree-Fock,” *J Phys G Nucl Part Phys*, vol. 38, no. 3, p. 033101, jan 2011. [Online]. Available: <https://doi.org/10.1088/0954-3899/2F38%2F3%2F033101>
- [10] J. Erler, N. Birge, M. Kortelainen, W. Nazarewicz, E. Olsen, A. Perhac, and M. Stoitsov, “The limits of the nuclear landscape,” *Nature*, vol. 486, p. 509, 2012. [Online]. Available: <https://www.nature.com/articles/nature11188>
- [11] M. Bender, R. Bernard, G. Bertsch, S. Chiba, J. Dobaczewski, N. Dubray, S. A. Giuliani, K. Hagino, D. Lacroix, Z. Li, P. Magierski, J. Maruhn, W. Nazarewicz, J. Pei, S. Péru, N. Pillet, J. Randrup, D. Regnier, P.-G. Reinhard, L. M. Robledo, W. Ryssens, J. Sadhukhan, G. Scampier, N. Schunck, C. Simenel, J. Skalski, I. Stetcu, P. Stevenson, S. Umar, M. Verriere, D. Vretenar, M. Warda, and S. Åberg, “Future of nuclear fission theory,” *J. Phys. G*, vol. 47, no. 11, p. 113002, oct 2020. [Online]. Available: <https://doi.org/10.1088/1361-6471/abab4f>
- [12] M. Stoitsov, J. Dobaczewski, W. Nazarewicz, and P. Ring, “Axially deformed solution of the Skyrme–Hartree–Fock–Bogolyubov equations using the transformed harmonic oscillator basis. the program HFBTHO (v1.66p),” *Comput. Phys. Commun.*, vol. 167, no. 1, pp. 43 – 63, 2005. [Online]. Available: <http://www.sciencedirect.com/science/article/pii/S0010465505000305>
- [13] R. N. Perez, N. Schunck, R.-D. Lasserri, C. Zhang, and J. Sarich, “Axially deformed solution of the Skyrme–Hartree–Fock–Bogolyubov equations using the transformed harmonic oscillator basis (III) HFTHO (v3.00): A new version of the program,” *Comput. Phys. Commun.*, vol. 220, pp. 363–375, 2017. [Online]. Available: <https://www.sciencedirect.com/science/article/pii/S0010465517302047>
- [14] J. Dobaczewski and J. Dudek, “Solution of the Skyrme-Hartree-Fock equations in the cartesian deformed harmonic oscillator basis I. The method,” *Comput. Phys. Commun.*, vol. 102, no. 1, pp. 166 – 182, 1997. [Online]. Available: <http://www.sciencedirect.com/science/article/pii/S0010465597000040>
- [15] N. Schunck, J. Dobaczewski, W. Satuła, P. Bączyk, J. Dudek, Y. Gao, M. Konieczka, K. Sato, Y. Shi, X. Wang, and T. Werner, “Solution of the Skyrme-Hartree–Fock–Bogolyubov equations in the Cartesian deformed harmonic-oscillator basis. (VIII) HFODD (v2.73y): A new version of the program,” *Comput. Phys. Commun.*, vol. 216, pp. 145–174, 2017. [Online]. Available: <https://www.sciencedirect.com/science/article/pii/S0010465517300942>
- [16] J. J. Dobaczewski, P. Bączyk, P. Becker, M. Bender, K. Bennaceur, J. Bonnard, Y. Gao, A. Idini, M. Konieczka, M. Kortelainen, and et al., “Solution of universal nonrelativistic nuclear DFT equations in the Cartesian deformed harmonic-oscillator basis. (IX) HFODD (3.06h): a new version of the program,” *J. Phys. G*, 2021. [Online]. Available: <http://dx.doi.org/10.1088/1361-6471/ac0a82>
- [17] M. Stoitsov, N. Michel, and K. Matsuyanagi, “New efficient method for performing Hartree-Fock-Bogoliubov calculations for weakly bound nuclei,” *Phys. Rev. C*, vol. 77, p. 054301, May 2008. [Online]. Available: <https://link.aps.org/doi/10.1103/PhysRevC.77.054301>
- [18] K. Bennaceur and J. Dobaczewski, “Coordinate-space solution of the Skyrme–Hartree–Fock–Bogolyubov equations within spherical symmetry. the program HFBRAD (v1.00),” *Comput. Phys. Commun.*, vol. 168, no. 2, pp. 96 – 122, 2005. [Online]. Available: <http://www.sciencedirect.com/science/article/pii/S0010465505002304>
- [19] J. C. Pei, M. V. Stoitsov, G. I. Fann, W. Nazarewicz, N. Schunck, and F. R. Xu, “Deformed coordinate-space Hartree-Fock-Bogoliubov approach to weakly bound nuclei and large deformations,” *Phys. Rev. C*, vol. 78, p. 064306, Dec 2008. [Online]. Available: <https://link.aps.org/doi/10.1103/PhysRevC.78.064306>
- [20] P.-G. Reinhard, B. Schuetrumpf, and J. Maruhn, “The Axial Hartree–Fock + BCS Code SkyAx,” *Comput. Phys. Commun.*, vol. 258, p. 107603, 2021. [Online]. Available: <http://www.sciencedirect.com/science/article/pii/S0010465520302927>
- [21] J. Maruhn, P.-G. Reinhard, P. Stevenson, and A. Umar, “The TDHF code Sky3D,” *Comput. Phys. Commun.*, vol. 185, no. 7, pp. 2195 – 2216, 2014. [Online]. Available: <http://www.sciencedirect.com/science/article/pii/S0010465514001313>

- [22] B. Schuettrumpf, P.-G. Reinhard, P. Stevenson, A. Umar, and J. Maruhn, "The TDHF code Sky3D version 1.1," *Comput. Phys. Commun.*, vol. 229, pp. 211 – 213, 2018. [Online]. Available: <http://www.sciencedirect.com/science/article/pii/S0010465518300845>
- [23] P.-G. Reinhard, "Skyrme-Hartree-Fock calculations of the nuclear ground state," in *Computational Nuclear Physics I - Nuclear Structure*, K. Langanke, S. Koonin, and J. Maruhn, Eds. Berlin: Springer, 1991, p. 28.
- [24] P.-G. Reinhard, "HFB solvers Sky1D and Sky2D", unpublished, 2021.
- [25] P. Bonche, H. Flocard, and P. Heenen, "Solution of the Skyrme HF+BCS equation on a 3D mesh," *Comput. Phys. Commun.*, vol. 171, no. 1, pp. 49–62, 2005. [Online]. Available: <https://www.sciencedirect.com/science/article/pii/S0010465505002821>
- [26] W. Ryssens, V. Hellemaans, M. Bender, and P.-H. Heenen, "Solution of the Skyrme-HF+BCS equation on a 3D mesh, II: a new version of the Ev8 code," *Comput. Phys. Commun.*, vol. 187, pp. 175–194, 2015. [Online]. Available: <https://www.sciencedirect.com/science/article/pii/S0010465514003361>
- [27] Ryssens, W., Bender, M., and Heenen, P. -H., "Iterative approaches to the self-consistent nuclear energy density functional problem - Heavy ball dynamics and potential preconditioning," *Eur. Phys. J. A*, vol. 55, no. 6, p. 93, 2019. [Online]. Available: <https://doi.org/10.1140/epja/i2019-12766-6>
- [28] G. Scamps, S. Goriely, E. Olsen, M. Bender, and W. Ryssens, "Grid Skyrme functional obtained using a committee of multilayer neural networks," 2021.
- [29] J. C. Pei, G. I. Fann, R. J. Harrison, W. Nazarewicz, Y. Shi, and S. Thornton, "Adaptive multi-resolution 3D Hartree-Fock-Bogoliubov solver for nuclear structure," *Phys. Rev. C*, vol. 90, p. 024317, Aug 2014. [Online]. Available: <https://link.aps.org/doi/10.1103/PhysRevC.90.024317>
- [30] S. Jin, K. J. Roche, I. Stetcu, I. Abdurrahman, and A. Bulgac, "The LISE package: Solvers for static and time-dependent superfluid local density approximation equations in three dimensions," *Comput. Phys. Commun.*, vol. 269, p. 108130, 2021. [Online]. Available: <https://www.sciencedirect.com/science/article/pii/S0010465521002423>
- [31] S. Jin, A. Bulgac, K. Roche, and G. Wlazlowski, "Coordinate-space solver for superfluid many-fermion systems with the shifted conjugate-orthogonal conjugate-gradient method," *Phys. Rev. C*, vol. 95, p. 044302, Apr 2017. [Online]. Available: <https://link.aps.org/doi/10.1103/PhysRevC.95.044302>
- [32] Y. Kashiwaba and T. Nakatsukasa, "Coordinate-space solver for finite-temperature Hartree-Fock-Bogoliubov calculations using the shifted Krylov method," *Phys. Rev. C*, vol. 101, p. 045804, Apr 2020. [Online]. Available: <https://link.aps.org/doi/10.1103/PhysRevC.101.045804>
- [33] N. Michel, K. Matsuyanagi, and M. Stoitsov, "Gamow-Hartree-Fock-Bogoliubov method: Representation of quasiparticles with Berggren sets of wave functions," *Phys. Rev. C*, vol. 78, p. 044319, Oct 2008. [Online]. Available: <https://link.aps.org/doi/10.1103/PhysRevC.78.044319>
- [34] J. C. Pei, A. T. Kruppa, and W. Nazarewicz, "Quasiparticle continuum and resonances in the Hartree-Fock-Bogoliubov theory," *Phys. Rev. C*, vol. 84, p. 024311, Aug 2011. [Online]. Available: <https://link.aps.org/doi/10.1103/PhysRevC.84.024311>
- [35] P.-G. Reinhard, M. Bender, K. Rutz, and J. A. Maruhn, "An HFB scheme in natural orbitals," *Z. Phys., A Hadrons nucl.*, vol. 358, no. 3, pp. 277–278, 1997. [Online]. Available: <https://link.springer.com/article/10.1007%2Fs002180050328>
- [36] N. Tajima, "Canonical-basis solution of the Hartree-Fock-Bogoliubov equation on a three-dimensional Cartesian mesh," *Phys. Rev. C*, vol. 69, p. 034305, Mar 2004. [Online]. Available: <https://link.aps.org/doi/10.1103/PhysRevC.69.034305>
- [37] M. Afibuzzaman, B. Schuettrumpf, and H. M. Aktulga, "Scalable nuclear density functional theory with Sky3D," *Comput. Phys. Commun.*, vol. 223, pp. 34 – 44, 2018. [Online]. Available: <http://www.sciencedirect.com/science/article/pii/S0010465517303491>
- [38] P. Ring and P. Schuck, *The nuclear many-body problem*. Springer-Verlag, Berlins, 2004.
- [39] J. Dobaczewski, W. Nazarewicz, and P.-G. Reinhard, "Pairing interaction and self-consistent densities in neutron-rich nuclei," *Nucl. Phys. A*, vol. 693, no. 1, pp. 361–373, 2001. [Online]. Available: <https://www.sciencedirect.com/science/article/pii/S0375947401009939>
- [40] P. Klüpfel, P.-G. Reinhard, T. J. Bürvenich, and J. A. Maruhn, "Variations on a theme by Skyrme: A systematic study of adjustments of model parameters," *Phys. Rev. C*, vol. 79, p. 034310, Mar 2009. [Online]. Available: <https://link.aps.org/doi/10.1103/PhysRevC.79.034310>
- [41] V. Blum, G. Lauritsch, J. Maruhn, and P.-G. Reinhard, "Comparison of coordinate-space techniques in nuclear mean-field calculations," *J. Comput. Phys.*, vol. 100, no. 2, pp. 364 – 376, 1992. [Online]. Available: <http://www.sciencedirect.com/science/article/pii/002199919290242Q>
- [42] R. W. Hockney, "Potential calculation and some applications," *Methods Comput. Phys.*, vol. 9, pp. 135–211, 1970.
- [43] J. Eastwood and D. Brownrigg, "Remarks on the solution of Poisson's equation for isolated systems," *J. Comput. Phys.*, vol. 32, no. 1, pp. 24–38, 1979. [Online]. Available: <https://www.sciencedirect.com/science/article/pii/0021999179901396>
- [44] M. Frigo and S. Johnson, "The design and implementation of FFTW3," *Proc. IEEE*, vol. 93, no. 2, pp. 216–231, 2005.
- [45] P.-G. Reinhard and R. Cusson, "A comparative study of Hartree-Fock iteration techniques," *Nucl. Phys. A*, vol. 378, no. 3, pp. 418 – 442, 1982. [Online]. Available: <http://www.sciencedirect.com/science/article/pii/0375947482904584>
- [46] P. J. Borycki, J. Dobaczewski, W. Nazarewicz, and M. V. Stoitsov, "Pairing renormalization and regularization within the local density approximation," *Phys. Rev. C*, vol. 73, p. 044319, Apr 2006. [Online]. Available: <https://link.aps.org/doi/10.1103/PhysRevC.73.044319>
- [47] P. Bonche, H. Flocard, P. Heenen, S. Krieger, and M. Weiss, "Self-consistent study of triaxial deformations: Application to the isotopes of Kr, Sr, Zr and Mo," *Nucl. Phys. A*, vol. 443, no. 1, pp. 39 – 63, 1985. [Online]. Available: <http://www.sciencedirect.com/science/article/pii/0375947485903203>
- [48] S. Krieger, P. Bonche, H. Flocard, P. Quentin, and M. Weiss, "An improved pairing interaction for mean field calculations using Skyrme potentials," *Nucl. Phys. A*, vol. 517, no. 2, pp. 275–284, 1990. [Online]. Available: <https://www.sciencedirect.com/science/article/pii/037594749090035K>
- [49] W. H. Press, S. A. Teukolsky, W. T. Vetterling, and B. P. Flannery, *Numerical Recipes in C: The Art of Scientific Computing*, 2nd ed. New York: Cambridge University Press, 1992.
- [50] S. G. Johnson, "Notes on FFT-based differentiation." [Online]. Available: <https://math.mit.edu/~stevenj/fft-deriv.pdf>
- [51] E. Chabanat, P. Bonche, P. Haensel, J. Meyer, and R. Schaeffer, "A Skyrme parametrization from subnuclear to neutron star densities Part II. Nuclei far from stabilities," *Nucl. Phys. A*, vol. 635, no. 1, pp. 231 – 256, 1998. [Online]. Available: <http://www.sciencedirect.com/science/article/pii/S0375947498001808>
- [52] T. Papenbrock and G. F. Bertsch, "Pairing in low-density Fermi gases," *Phys. Rev. C*, vol. 59, pp. 2052–2055, Apr 1999. [Online]. Available: <https://link.aps.org/doi/10.1103/PhysRevC.59.2052>
- [53] M. Bender, K. Rutz, P. Reinhard, and J. Maruhn, "Pairing gaps from nuclear mean-field models," *Eur. Phys. J. A*, vol. 8, 05 2000. [Online]. Available: <https://doi.org/10.1007/s10050-000-4504-z>
- [54] B. Schuettrumpf, W. Nazarewicz, and P.-G. Reinhard, "Time-dependent density functional theory with twist-averaged boundary conditions," *Phys. Rev. C*, vol. 93, p. 054304, May 2016. [Online]. Available: <https://link.aps.org/doi/10.1103/PhysRevC.93.054304>
- [55] R. J. Furnstahl, G. Hagen, and T. Papenbrock, "Corrections to nuclear energies and radii in finite oscillator spaces," *Phys. Rev. C*, vol. 86, p. 031301, Sep 2012. [Online]. Available: <https://link.aps.org/doi/10.1103/PhysRevC.86.031301>
- [56] S. Binder, A. Ekström, G. Hagen, T. Papenbrock, and K. A. Wendt, "Effective field theory in the harmonic oscillator basis," *Phys. Rev. C*, vol. 93, p. 044332, Apr 2016. [Online]. Available: <https://link.aps.org/doi/10.1103/PhysRevC.93.044332>
- [57] S. N. More, A. Ekström, R. J. Furnstahl, G. Hagen, and T. Papenbrock, "Universal properties of infrared oscillator basis extrapolations," *Phys. Rev. C*, vol. 87, p. 044326, Apr 2013. [Online]. Available: <https://link.aps.org/doi/10.1103/PhysRevC.87.044326>
- [58] N. Nikolov, N. Schunck, W. Nazarewicz, M. Bender, and J. Pei, "Surface symmetry energy of nuclear energy density functionals," *Phys. Rev. C*, vol. 83, p. 034305, Mar 2011. [Online]. Available: <https://link.aps.org/doi/10.1103/PhysRevC.83.034305>
- [59] N. Schunck, "Density functional theory approach to nuclear fission," *Acta Phys. Pol. B*, vol. 44, no. 3, p. 263, 2013. [Online]. Available:

<http://dx.doi.org/10.5506/APhysPolB.44.263>